Palaeogeography, Palaeoclimatology, Palaeoecology 609 (2023) 111311

Contents lists available at ScienceDirect

Palaeogeography, Palaeoclimatology, Palaeoecology

journal homepage: www.elsevier.com/locate/palaeo

The structure of marine isotope Stage 11 and its alignment with the Holocene

Yong Wang [a], Xunlin Yang [a,b,*], Yongjin Wang [c], Quan Wang [d], R. Lawrence Edwards [e]

[a] Key Laboratory of Karst Environment, School of Geographical Sciences, Southwest University, Chongqing 400715, China
[b] Jinfo Mountain Karst Ecosystem National Observation and Research Station, Southwest University, Chongqing 400715, China
[c] School of Geography, Nanjing Normal University, Nanjing 210097, China
[d] Chongqing Key Laboratory of Earth Surface Processes and Environmental Remote Sensing in Three Gorges Reservoir Area, Chongqing Normal University, Chongqing 401331, China
[e] Department of Earth Sciences, University of Minnesota, Minneapolis, MN 55455, USA

ARTICLE INFO

Editor: M Elliot

Keywords:
Marine isotope stage 11
Holocene
Asian summer monsoon
Stalagmite
Southwest China

ABSTRACT

Marine Isotope Stage 11 (MIS 11) has long been used to estimate the natural length of the present Holocene interglacial, due to their similarity in terms of astronomically-driven insolation variations. It is debated, however, which part of MIS 11 should be aligned to the Holocene, according to different alignment strategies. Here, we use a well-dated, high-resolution Asian summer monsoon (ASM) record covering the whole of MIS 11 (from 445 to 320 thousand years ago (ky)) from stalagmite J33 from Jinfo Cave in Southwest China, to attempt to resolve the issue. The oxygen isotope ($\delta^{18}O$) record of stalagmite J33 enables MIS 11 to be divided into 5 stages: MIS 11a–11e. Among them, MIS 11a, MIS 11c and MIS 11e are relatively strong monsoon periods, while MIS 11b and MIS 11d are relatively weak monsoon periods. According to the similarities and differences of Earth orbital parameters between MIS 11 and MIS 1, we propose a new alignment strategy in which the interglacial maxima and their preceding glacial terminations can be aligned. This new comparison scheme shows that the "missing" parts of the Holocene correspond to MIS 11d and MIS 11e, which explains why the MIS 11 interglacial period was longer than the current Holocene interglacial.

1. Introduction

The Holocene (Marine Isotope Stage 1 (MIS 1)) has lasted for more than 11.6 ky, and its duration has exceeded the shortest interglacial period in the past (Kukla, 2003; Tzedakis et al., 2012). Given its significance for humanity, it is clearly important to estimate the timing of the end of the Holocene and the beginning of the next glacial period (EPICA community members, 2004; Kukla, 2003; Loutre and Berger, 2003). Comparison with Earth orbital parameters suggests that MIS 11 (425–360 thousand years before present (ky BP)) is a close analog of the current interglacial period and therefore it is highly significant for studies of future climate change (EPICA community members, 2004; Loutre and Berger, 2000, 2003; Masson-Delmotte et al., 2006; Ruddiman, 2005; Tzedakis, 2010; Zhao et al., 2019). Though there are obvious similarities in insolation characteristics between MIS 1 and 11, the climatic structure and patterns of MIS 11 in many paleoclimatic records are very different from those of MIS 1 (EPICA community members, 2004); and thus, there is much debate about how best to align the Holocene with MIS 11 (Candy et al., 2014; Ruddiman, 2005; Tierney et al., 2020). However, the unusually long length of the MIS 11 interglacial makes it difficult to correlate it with the current interglacial (Cheng et al., 2016; Mcmanus et al., 1999; Tzedakis et al., 2012). If human impacts are ignored, then the lengths of the current interglacial period obtained by different alignments are very different. Based on the Earth orbital precession signal, the Holocene can be aligned with the latest part of MIS 11c (Ruddiman, 2005), implying that the current interglacial period should have ended, and a cooling trend commenced. In this way, the occurrence times of the insolation maximum and the interglacial maximum are aligned, but the deglacial period and the termination point are misaligned to different degrees. The Holocene and early MIS 11 can be aligned based on the preceding termination (or Earth orbital obliquity signal), which means the current interglacial will last for another ~10–16 ky. This alignment causes precession (or insolation) to be almost out-of-phase, but nevertheless there are close similarities

* Corresponding author at: Key Laboratory of Karst Environment, School of Geographical Sciences, Southwest University, Chongqing 400715, China.
E-mail address: xlyang@swu.edu.cn (X. Yang).

https://doi.org/10.1016/j.palaeo.2022.111311
Received 7 June 2022; Received in revised form 22 September 2022; Accepted 2 November 2022
Available online 9 November 2022

between the paleotemperature and greenhouse gas records of MIS 1 and the early part of MIS 11.

The internal structure and duration of MIS 11 are much debated in paleoclimatology (Bassinot et al., 1994; Railsback et al., 2015; Prokopenko et al., 2001). The initial SPECMAP studies (Imbrie et al., 1984) showed that the substages of MIS 11 include the relatively warm MIS 11a and MIS 11c and the relatively cold MIS 11b. The biogenic silica record from Lake Baikal, from the northern border of the Asian monsoon region, shows that MIS 11 has three relatively warm intervals: MIS 11a, 11c and 11e (Prokopenko et al., 2001). Various records now demonstrate that the end of MIS 11 was punctuated by multiple millennial-scale stadial and interstadial events (Mcmanus et al., 1999; EPICA community members, 2004; Prokopenko et al., 2001; Voelker et al., 2010; Palumbo et al., 2013). Investigating the details of this climatic complexity during MIS 11 can potentially increase our understanding of the structure of this warm stage. The Asian summer monsoon (ASM) is an important component of atmospheric circulation and plays a major role in global hydrological and energy cycles (Wang et al., 2008; Cheng et al., 2016). The Chinese stalagmite record has greatly increased our knowledge of the variations of the Asian monsoon on different time scales, and it is a valuable supplement to the paleoclimate records provided by marine sediments, ice cores, and loess deposits (Cheng et al., 2016; EPICA community members, 2004; Prokopenko et al., 2001). In this study we use paleoclimate records from Jinfo Cave in Southwest China to study the climatic structure and ASM changes during MIS 11. From the perspective of the ASM, this high-resolution and absolutely-dated record enables us to assess the utility of MIS 11 as a natural analogue of the current interglacial period.

2. Materials and methods

Jinfo Cave (29°01′ N, 107°11′ E) is 85 km southeast of Chongqing city, in Southwest China, at an elevation of 2114 m (Fig. 1). The local meteorological monitoring data for five consecutive years (2012–2016) show that the climate at the cave site is dominated by the ASM, with the mean annual temperature of 8.1 °C and mean annual precipitation of 1384 mm (Chen and Li, 2018). One stalagmite (J33) from Jinfo Cave, ~50 mm wide and 397 mm long (Fig. 2), was precisely dated using ^{230}Th techniques. For U—Th dating, subsamples (0.5–1 g) of stalagmite J33 were cut along the laminations. All subsamples were ultrasonicated with deionized water 4–5 times until there was no visible powder or detrital material, and then dried at 70 °C. From a total of 19 subsamples, 13 ^{230}Th ages were determined at the High-Precision Mass Spectrometry and Environmental Change Laboratory (HISPEC), National Taiwan University, and an additional 6 ^{230}Th ages were determined at the Minnesota Isotope Laboratory, University of Minnesota, USA. All measurements were made on Thermo-Finnigan Neptune multi-collector inductively coupled plasma mass spectrometers, using a recently improved technique (Cheng et al., 2013; Jaffey et al., 1971; Shen et al., 2012).

For stable isotope measurements, 80–100 μg of powdered sample was obtained using a 0.3-mm-diameter carbide dental bur applied to the smoothed surface, parallel to the central growth axis. The powder was analyzed using an online, automated carbonate preparation system (Kiel III) linked to a Finnigan MAT-253 ratio mass spectrometer at the Isotope Laboratory of Nanjing Normal University and Southwest University, China. Standards (NBS19) were run every 9 measurements to check the reproducibility. The precision of the δ^{18}O measurements is ±0.06‰ at the 1σ level.

3. Results

The chronology of stalagmite J33 was established by linear interpolation between successive ^{230}Th ages (Table 1, Fig. 2), and this chronology was used to produce a stalagmite δ^{18}O time series (Table S1). The cave δ^{18}O record is generally in accord with changes in mid-July Northern Hemisphere summer insolation (Laskar et al., 2004), as shown in Fig. 3. A total of 2004 carbon and oxygen isotope values were obtained, with a resolution of 50 years, with the age range of 365–442 ky BP. The average stalagmite δ^{18}O value is −7.30‰, and the minimum, maximum, and range are −9.03‰, −4.08‰, and 4.95‰, respectively.

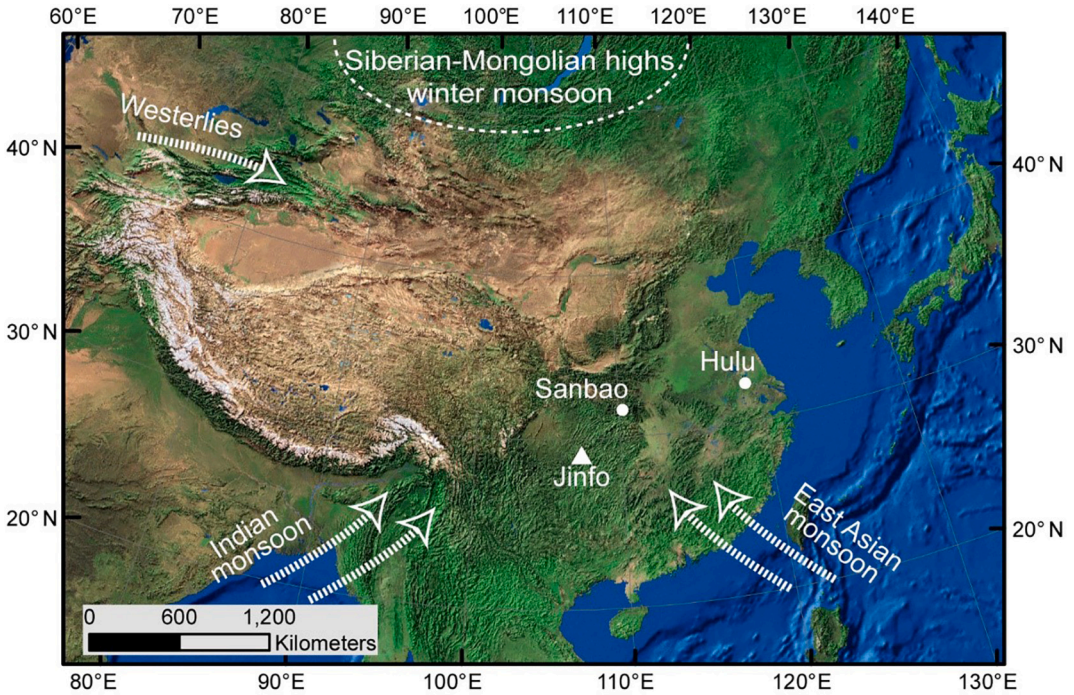

Fig. 1. Map showing the caves investigated and mentioned in this study: Jinfo (29°01′N, 107°11″E), Sanbao Cave (31°40′N, 110°26′E) (Wang et al., 2008; Cheng et al., 2016) and Hulu Cave (32°30′N, 119°10′E) (Wang et al., 2001). Arrows schematically indicate wind directions of the Asian monsoon circulation and the westerlies. The three cave locations are predominantly influenced by the monsoon climate.

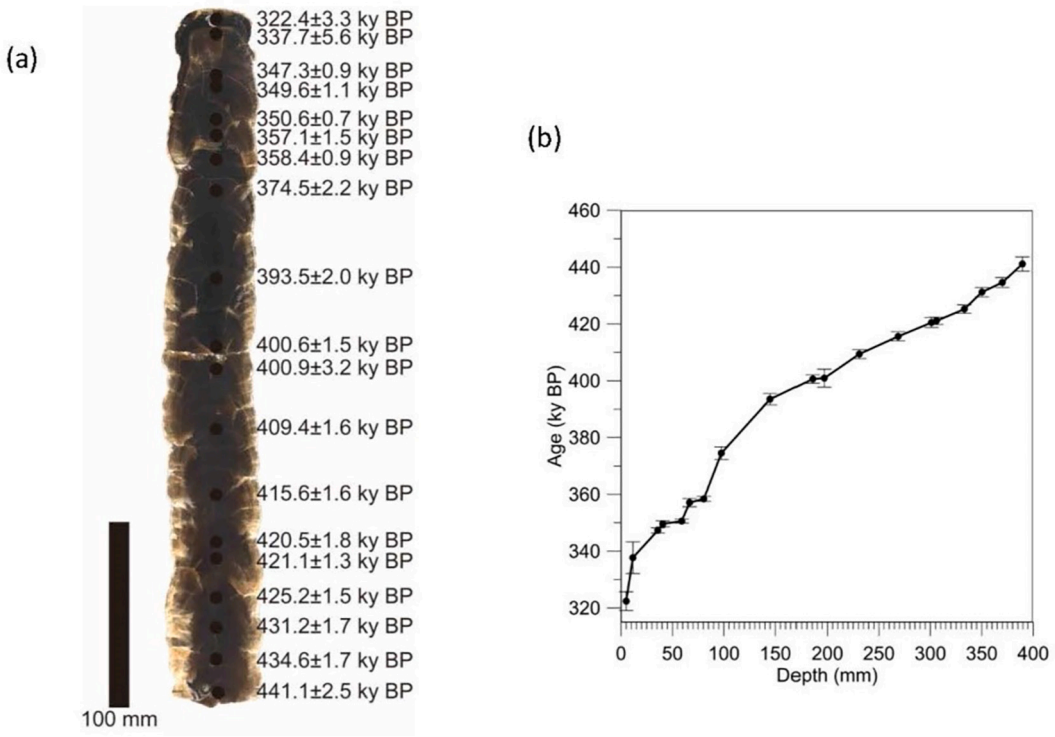

Fig. 2. The polished surface of slabbed J33 with dots representing ^{230}Th dating results (Fig. 2(a)) and age models for stalagmite J33 (Fig. 2(b)). The chronology of stalagmite J33 was established by linear interpolation between successive ^{230}Th dates. The vertical error bars depict errors (2σ) of the ^{230}Th dates.

Before interpreting a stalagmite $\delta^{18}O$ record as a climatic proxy, it is necessary to confirm that the calcite was deposited under isotopic equilibrium fractionation conditions (Hendy, 1971). Hendy (1971) proposed a scheme for assessing the isotopic equilibrium fractionation between precipitated calcium carbonate and the parent solution. Based on the principles of Hendy (1971), there is no obvious correlation (N = 2004, R = 0.05) between the $\delta^{18}O$ and $\delta^{13}C$ values of stalagmite J33 (Fig. S1), which suggests that stalagmite J33 was precipitated close to isotopic equilibrium conditions, and that the $\delta^{18}O$ signal is primarily of climatic origin. A replication test is another robust means for assessing isotopic equilibrium fractionation (Dorale and Liu, 2009). A comparison of the J33 record with three stalagmite records from Sanbao Cave (Cheng et al., 2016) reveals a high degree of similarity among the main trends of their $\delta^{18}O$ records (Fig. 3). Since the stalagmite records are nearly identical, they can be regarded as reliable proxies of ASM strength at the regional scale (Cheng et al., 2016; Wang et al., 2008).

The timing of Termination V (T-V) in the stalagmite J33 record is 3 ky younger than in the Sanbao records. The stalagmite J33 record has only 3 age data near Termination V (420.5 ± 1.8 ky BP, 421.1 ± 1.3ky BP and 425.5 ± 1.5ky BP), while the Sanbao records have 16 precise age constraints for Termination V, with the minimum age error of ±0.88 ky. Moreover, the ASM variations recorded at Sanbao Cave can be correlated with both marine and cave sequences across a wide geographical range (Clemens et al., 2018; Cheng et al., 2016). For the above reasons and given the near-identical dates for the anomalously weak ASM event prior to T-V in the three records from Sanbao Cave, we tuned the stalagmite J33 record to the Sanbao chronology for this older period (Fig. S2).

4. Discussion

4.1. Interpretation of the $\delta^{18}O$ signal of stalagmites

Because of the influence of the water vapor source, depositional processes, and ventilation conditions, the climatic significance of stalagmites in the ASM region is complex, resulting in much controversy. Interpretations of stalagmite $\delta^{18}O$ records in the ASM region can be classified into two types: (Bassinot et al., 1994) Stalagmite $\delta^{18}O$ values reflect ASM intensity/precipitation (Cheng et al., 2016; Wang et al., 2008; Yang et al., 2019; Yuan et al., 2004; Zhang et al., 2008); (Mills et al., 2020) stalagmite $\delta^{18}O$ values reflect the proportion of different water vapor sources (Maher, 2008; Tan, 2009). Based on 14 cave records, Yang et al. (2019) concluded that the principal modes of variation of the Holocene stalagmite $\delta^{18}O$ records were similar throughout the Asian monsoon domain, and they proposed that stalagmite $\delta^{18}O$ sequences reflect changes in ASM intensity, rather than local precipitation amount. Due to the large spatial differences in monsoon precipitation, Cheng et al. (2019) further pointed out that multiple modes of variation may exist in reconstructions of seasonal inter-annual or Holocene precipitation variations from different locations in the same monsoon system. Modern cave monitoring of Mt. Jinfo showed that changes in precipitation $\delta^{18}O$ are closely related to atmospheric circulation patterns on inter-annual time scales (Chen and Li, 2018). Recently, Cheng et al. (2021) concluded that stalagmite $\delta^{18}O$ data can be interpreted as a proxy for ASM intensity, with low values indicating a strong ASM, and vice versa.

4.2. Climatic structure of MIS 11

The internal structure and duration of MIS 11 are much debated (Bassinot et al., 1994; Railsback et al., 2015; Prokopenko et al., 2001). The high-resolution stalagmite J33 record from Jinfo Cave provides detailed insights into the internal structure and climatic events of MIS 11 on a fine time scale. It is widely accepted that T-V was the end of the MIS 12 glacial period and the beginning of MIS 11 (Mcmanus et al., 1999; Prokopenko et al., 2001; Voelker et al., 2010), as defined by a stacked marine $\delta^{18}O$ record (Lisiecki and Raymo, 2005). The J33 stalagmite record has a large positive shift in $\delta^{18}O$ centered at 427 ky BP, which represents an extremely weak monsoon interval during T-V, and it shows that T-V ended at ~425 ky BP, implying the onset of MIS 11. According

Table 1
^{230}Th date results for stalagmite J33 from Jinfo Cave, China.

Sample Number	Depth (mm to top)	^{238}U (ppb)	^{232}Th (ppt)	^{230}Th / ^{232}Th (atomic x10^{-6})	δ^{234}U (measured)	^{230}Th / ^{238}U (activity)	Age (ky BP) (uncorrected)	Age (ky BP) (corrected)	$\delta^{234}U_{Initial}$ (corrected)
J33–1	5.0	3390.1 ± 4.3	369.0 ± 21.5	255,546.7 ± 14,872.0	587.5 ± 1.7	1.687 ± 0.003	322.4 ± 3.3	322.4 ± 3.3	1459.2 ± 14.3
J33–2	11.5	2650.1 ± 5.0	649.6 ± 20.8	114,429.9 ± 3664.1	585.2 ± 2.8	1.701 ± 0.005	337.7 ± 5.6	337.7 ± 5.6	1518.0 ± 25.2
J33–3	35.8	2883.6 ± 0.1	1509.5 ± 9.7	52,322.4 ± 337.6	546.6 ± 0.2	1.661 ± 0.001	347.4 ± 0.9	347.3 ± 0.9	1456.8 ± 3.8
J33–4	40.6	2641.0 ± 0.2	276.2 ± 9.8	261,324.4 ± 9240.2	541.9 ± 0.3	1.657 ± 0.001	349.6 ± 1.1	349.6 ± 1.1	1453.7 ± 4.5
J33–5	59.0	3104.9 ± 7.6	432.5 ± 1.1	198,226.0 ± 53.0	554.8 ± 0.4	1.675 ± 0.000	350.6 ± 0.7	350.6 ± 0.7	1492.0 ± 3.2
J33–6	66.7	2553.6 ± 0.1	244.2 ± 6.9	286,830.3 ± 8057.8	541.8 ± 0.2	1.664 ± 0.001	357.1 ± 1.5	357.1 ± 1.5	1484.1 ± 6.4
J33–7	80.5	3183.1 ± 0.2	557.2 ± 6.8	155,915.9 ± 1909.4	534.4 ± 0.3	1.655 ± 0.001	358.4 ± 0.9	358.4 ± 0.9	1469.5 ± 4.0
J33–8	97.6	2169.6 ± 0.1	1992.7 ± 8.6	28,650.9 ± 126.3	479.4 ± 0.3	1.596 ± 0.002	374.5 ± 2.2	374.5 ± 2.2	1379.3 ± 8.7
J33–9	144.9	2516.4 ± 0.1	884.9 ± 10.2	72,003.1 ± 832.5	424.5 ± 0.3	1.536 ± 0.001	393.5 ± 2.0	393.5 ± 2.0	1288.5 ± 7.5
J33–10	185.7	2875.4 ± 0.1	429.4 ± 10.7	167,329.4 ± 4184.0	406.4 ± 0.3	1.516 ± 0.001	400.6 ± 1.5	400.6 ± 1.5	1258.9 ± 5.3
J33–11	196.9	2158.7 ± 0.1	2182.9 ± 11.0	24,635.3 ± 127.0	402.8 ± 0.3	1.511 ± 0.002	400.9 ± 3.2	400.9 ± 3.2	1248.6 ± 11.2
J33–12	230.9	3113.8 ± 0.2	1397.6 ± 9.8	55,814.2 ± 391.3	406.0 ± 0.3	1.519 ± 0.001	409.4 ± 1.6	409.4 ± 1.6	1288.8 ± 5.9
J33–13	268.7	2791.5 ± 0.2	738.7 ± 28.7	95,730.9 ± 3715.6	416.4 ± 0.3	1.536 ± 0.001	415.6 ± 1.6	415.6 ± 1.6	1345.7 ± 6.1
J33–14	301.2	2906.0 ± 0.1	479.0 ± 8.4	154,689.1 ± 2718.8	422.2 ± 0.3	1.546 ± 0.001	420.5 ± 1.8	420.5 ± 1.8	1383.2 ± 7.1
J33–15	306.0	3621.9 ± 8.7	672.0 ± 1.6	137,821.0 ± 39.0	425.2 ± 0.3	1.551 ± 0.000	421.1 ± 1.3	421.1 ± 1.3	1395.4 ± 5.3
J33–16	333.0	3173.3 ± 7.7	607.6 ± 1.5	134,437.0 ± 38.0	431.6 ± 0.4	1.561 ± 0.000	425.2 ± 1.5	425.2 ± 1.5	1432.7 ± 6.2
J33–17	350.1	2564.7 ± 0.1	77.7 ± 7.4	856,787.2 ± 81,351.6	439.9 ± 0.3	1.575 ± 0.001	431.2 ± 1.7	431.2 ± 1.7	1485.4 ± 7.4
J33–18	370.0	3829.9 ± 10.5	255.1 ± 0.7	383,366.0 ± 123.0	419.2 ± 0.4	1.549 ± 0.001	434.6 ± 1.7	434.6 ± 1.7	1429.1 ± 6.9
J33–19	389.5	2437.6 ± 0.1	140.4 ± 10.0	441,569.5 ± 31,340.3	413.0 ± 0.3	1.543 ± 0.001	441.1 ± 2.5	441.1 ± 2.5	1434.1 ± 10.2

U decay constants: $l_{238} = 1.55125 \times 10^{-10}$ (Jaffey et al., 1971) and $l_{234} = 2.82206 \times 10^{-6}$ (Cheng et al., 2013). Th decay constant: $l_{230} = 9.1705 \times 10^{-6}$ (Cheng et al., 2013). $\delta^{234}U = ([234\ U/238\ U]_{activity} - 1) \times 1000$. $\delta^{234}U_{initial}$ was calculated based on the ^{230}Th age (T), i.e., $\delta^{234}U_{initial} = \delta^{234}U_{measured} \times e^{l_{234}T}$. Corrected ^{230}Th ages assume the initial ^{230}Th/^{232}Th atomic ratio of $4.4 \pm 2.2 \times 10^{-6}$. These are the values for a material at secular equilibrium, with the bulk earth ^{232}Th/^{238}U value of 3.8. The errors are arbitrarily assumed to be 50%. B.P. stands for "Before Present" where the "Present" is defined as the year 1950 CE.

to the stalagmite J33 record, the boundary between MIS 11 and MIS 10 can be set at 365 ky BP, which is consistent with the SPECMAP oxygen isotope stack (Imbrie et al., 1984) and a low-latitude stack (Bassinot et al., 1994). MIS 11, as recorded by the δ^{18}O record of stalagmite J33, lasted for ~60 ky, which is consistent with the traditional duration of MIS 11 (Palumbo et al., 2013). According to the subdivision scheme of Railsback et al. (2015), we divide MIS 11 in stalagmite J33 into five stages: MIS 11a –11e. Among them, MIS 11a, MIS 11c and MIS 11e are relatively strong monsoon periods, while MIS 11b and MIS 11d are relatively weak monsoon periods (Fig. 4). Additionally, MIS 11b can be divided into three substages: MIS 11b I, MIS 11b II, and MIS 11b III (Bassinot et al., 1994).

At the end of T-V, δ^{18}O in stalagmite J33 rapidly decreased by 3.50‰, indicating the abrupt strengthening of the monsoon, and the first short-term strong monsoon phase of MIS 11 began. This strong monsoon event lasted for only ~3 ky, and is identified as MIS 11e, which corresponds to the first small insolation peak in MIS 11 and the warm stage MIS 11e recorded in Lake Baikal (Prokopenko et al., 2001; Railsback et al., 2015). Subsequently, the stalagmite J33 δ^{18}O record gradually became more positive, which lasted for ~5 ky, suggesting a short weak monsoon stage corresponding to MIS 11d (Railsback et al., 2015).

After MIS 11d, the stalagmite J33 δ^{18}O record gradually became more negative again, and a large flat-topped plateau with more negative oxygen isotopes developed from ~405 ky BP, suggesting that the monsoon was relatively strong. This plateau corresponds to the MIS 11c interval of maximum temperature recorded at Lake Baikal (Prokopenko et al., 2001). After 401 ky BP, the stalagmite δ^{18}O values gradually became more positive and reached a local maximum with relatively positive values at ~397 ky BP, indicating the end of MIS 11c. The δ^{18}O values then remained relatively stable and more negative during the interval of 409–401 ky BP, indicating that the monsoon was strong, which represents the climatic optimum of MIS 11c (de Abreu et al., 2005; Ruddiman, 2005, 2007; Kandiano et al., 2017; Tzedakis et al., 2017). The duration of MIS 11c recorded by stalagmites is similar to that of the Holsteinian interglacial in Central and Eastern Europe (Koutsodendris et al., 2010).

The EPICA ice core record from Antarctica shows two warm peaks during MIS 11c (EPICA community members, 2004), separated by a cold event lasting ~7.7 ky. This cold event corresponds to the weak monsoon phase during MIS 11d recorded by stalagmites from monsoonal Asia. Railsback et al. (2015) proposed that the second peak (413–397 ky BP) of MIS 11c recorded by EPICA corresponds to the real MIS 11c because the temperature and methane content in the second peak exceed those of the first peak (EPICA community members, 2004; Jouzel et al., 2007). The second peak corresponds to the strongest monsoon during MIS 11c recorded by stalagmite J33.

Asian stalagmite records spanning the last 640 ky show that interglacial maxima corresponded to a strong ASM (Cheng et al., 2016). During interglacial periods, the Intertropical Convergence Zone moved northward, driven by insolation, and the ASM strengthened. The first

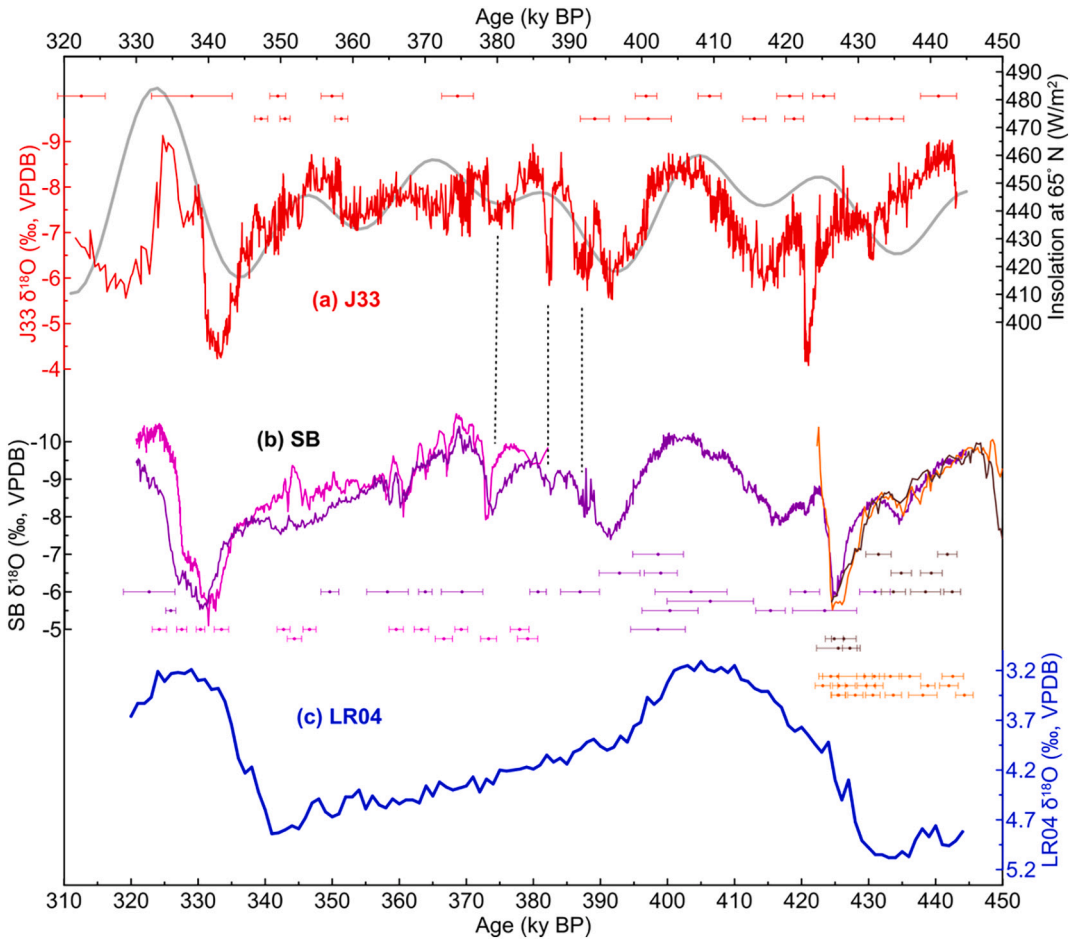

Fig. 3. Paleoclimatic records of MIS 11. (a). The $\delta^{18}O$ record of stalagmite J33 from Jinfo Cave in Southwest China, together with ^{230}Th dates (red dots with errors bars), overlapped with the curve of July 21 insolation at 65°N (Laskar et al., 2004) (grey). (b). Stalagmite $\delta^{18}O$ records from Sanbao Cave in Southwest China (Cheng et al., 2016), together with ^{230}Th dates (dots with errors bars). (c). stacked marine benthic $\delta^{18}O$ record (Lisiecki and Raymo, 2005). (For interpretation of the references to colour in this figure legend, the reader is referred to the web version of this article.)

insolation peak of MIS 11, corresponding to MIS 11e, is smaller than that of any interglacial maximum of the past 640 ky (Cheng et al., 2016); thus, MIS 11e may only be an interstadial episode (Tzedakis et al., 2017), rather than a full interglacial period, and definitely not an interglacial maximum. Additionally, the $\delta^{18}O$ record of stalagmite J33 during MIS 11c is ~1‰ lighter than that of MIS 11e. Therefore, based on the intensity and duration of the monsoon, MIS 11c can be defined as the true interglacial.

The second half of MIS 11 comprises four stages: MIS 11a, MIS 11b I, MIS 11b II, and MIS 11b III (397–365 ky BP), because precession variations during this interval were suppressed by the low eccentricity and thus the insolation changes were small and less clearly defined. After the end of MIS 11c, the $\delta^{18}O$ record of stalagmite J33 rapidly became positive and thus the monsoon weakened accordingly. Although there was a millennial-scale monsoon intensification event, the monsoon intensity was relatively weak during 397–390 ky BP (termed MIS 11b III), corresponding to the second insolation minimum of MIS 11. During the period of 390–365 ky BP, the stalagmite $\delta^{18}O$ values were generally negative, implying that the monsoon was strong, although the monsoon intensity was variable. This period was characterized by a series of millennial-scale weak monsoon events (WME). The timing of these WMEs agrees is consistent with those in the record from Sanbao Cave (Fig. 3) (Cheng et al., 2016), and they match the North Atlantic cold events and Antarctic warming events within the dating error range (EPICA community members, 2004; Martrat et al., 2007; Siddall et al., 2010). This synchronous phasing can be explained by a bipolar see-saw mechanism (Broecker, 1998; Voelker et al., 2010), whereby changes in the strength of the Atlantic meridional overturning circulation (AMOC) led to variations in inter- hemispheric heat transport. Both ice core and marine records demonstrate this climatic instability during the latter part of MIS 11 (EPICA community members, 2004; Martrat et al., 2007). The EPICA Dome C ice core record (EPICA community members, 2004) indicates three warm peaks after MIS 11c, which were interrupted by cold phases. Bassinot et al. (1994) showed that, following the main interglacial MIS 11c maximum, the low-latitude $\delta^{18}O$ record exhibits two interstadial/stadial cycles.

4.3. Alignment of MIS 11 and MIS 1

The previous alignment scheme mainly considered the similarities between MIS 11 and MIS 1, while ignoring the differences in orbital parameters and insolation. Both precession and obliquity affect insolation and glacial/interglacial cycles, and thus it is insufficient to consider only one of these parameters in an alignment scheme. Additionally, the past five glacial/interglacial cycles show that glacial terminations correspond to large-amplitude WMEs, and the interglacial optima correspond to stages of a strong and stable monsoon (Wang et al., 2008; Cheng et al., 2016). Therefore, according to the similarities and differences of astronomical parameters between the two stages and the characteristics of glacial/interglacial cycles, we propose to take precession (the insolation maximum) and the preceding termination as the starting point for the alignment (Fig. 5). In the Late Pleistocene, since the

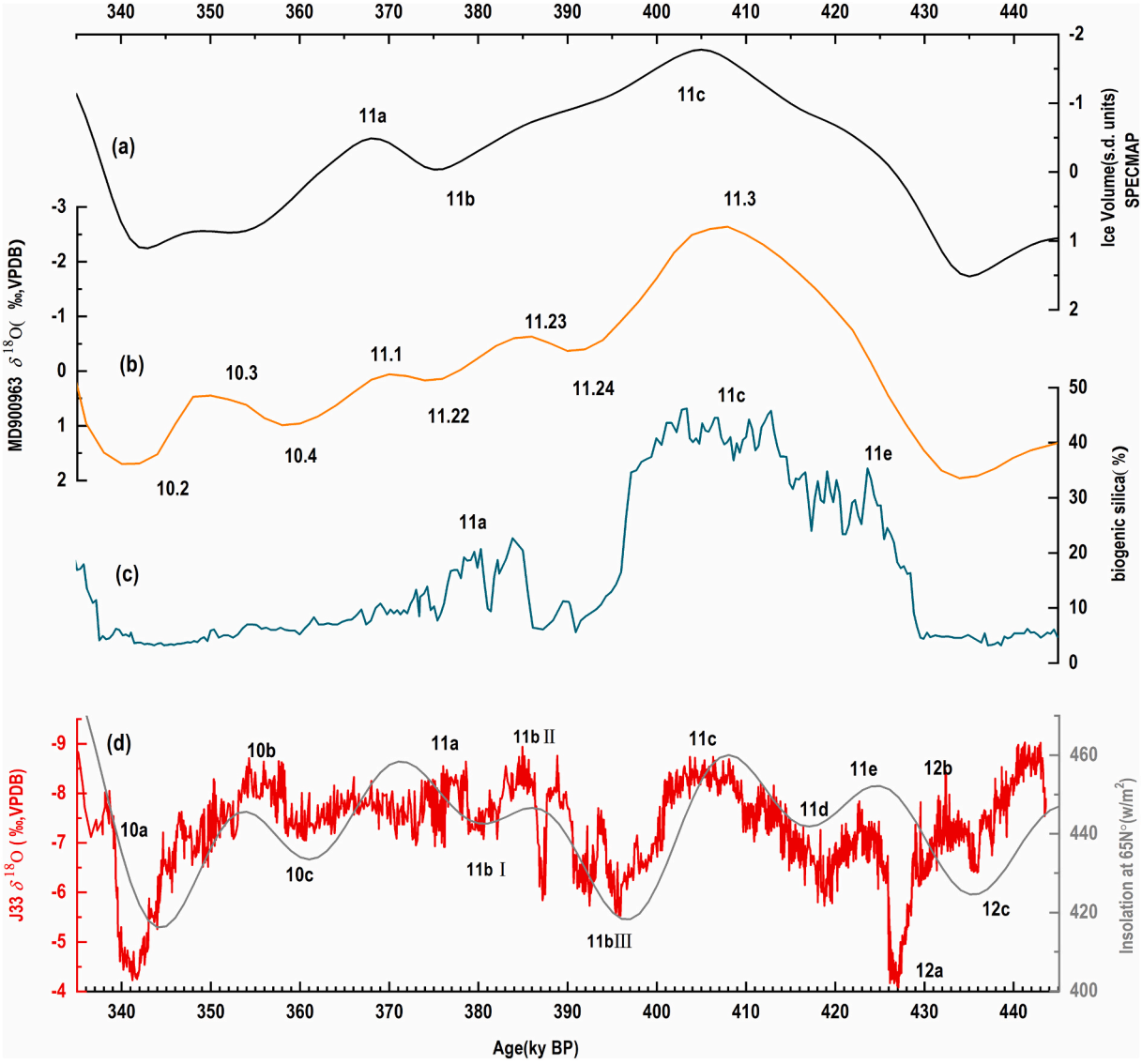

Fig. 4. The climatic structure of MIS 11. (a). SPECMAP $\delta^{18}O$ stack (Imbrie et al., 1984). (b). Low-latitude planktonic $\delta^{18}O$ record (SPECMAP units) (Bassinot et al., 1994). (c). Biogenic silica record from Lake Baikal (Prokopenko et al., 2001). (d). $\delta^{18}O$ record from stalagmite J33 overlapped with the curve of July 21 insolation at 65°N (Laskar et al., 2004).

obliquity cycle (41 ky) controlled the rhythm of Quaternary deglaciations (Huybers & Wunsch, 2005), the termination was a significant event at the end of each glacial/interglacial cycle. Considering that both MIS 11 and the Holocene correspond to intervals of low eccentricity, obliquity should exert the main climatic influence at these times. Therefore, it is important to align the preceding terminations, which also consider the contributions of millennial-scale events and obliquity.

As noted by Ruddiman (2007), the key difference between the two interglacials is the duration of their preceding terminations. Cheng et al. (2016) found that an anomalous millennial-scale climatic deterioration occurred during glacial terminations immediately before each interglacial period, at a time of increasing boreal summer insolation but when the terrestrial ice volume remained substantial. Combined with insolation forcing, this effect acts as a pacemaker of glacial terminations via a strong feedback with ice sheet instability (Denton et al., 2010). Each termination exhibited an extremely large WME associated with a large influx of ice-rafted detritus to the North Atlantic and a significant increase in Antarctic temperature and global atmospheric CO_2 concentration (Cheng et al., 2016). The exceptionally prolonged collapse of the AMOC (Stephen et al., 2009), coupled with a series of feedbacks in the bipolar see-saw model, has been regarded as the pacemaker of glacial terminations (Cheng et al., 2016; Denton et al., 2010). Hence, the duration of such an unusual event and its occurrence during a period of increasing insolation would result in differences in the duration and structure of each interglacial, as summarized by Tzedakis et al. (2012). This highlights the important role of glacial terminations in evaluating the utility of MIS 11 as an analog of the Holocene.

Milankovitch theory provides the basis for regarding MIS 11 as an analog of MIS 1 (Loutre and Berger, 2000; Ruddiman, 2005). These two interglacial periods have similar orbital parameters, resulting in similar insolation changes (Loutre and Berger, 2003). The alignment of MIS 11 and MIS 1 based on precession signals (Ruddiman, 2005) is straightforward in principle: the insolation maxima (interglacial optima) can be directly aligned.

Based on this new alignment scheme, we find that MIS 11d and MIS 11e, corresponding to the first precession cycle of MIS 11, lasted for ~13 ky, and there is no corresponding feature in the precession cycle of MIS 1. The current interglacial spans a single insolation maximum, while MIS 11 spanned two (weak) precession-driven insolation maxima separated by a minor minimum (Bassinot et al., 1994; Candy et al., 2014;

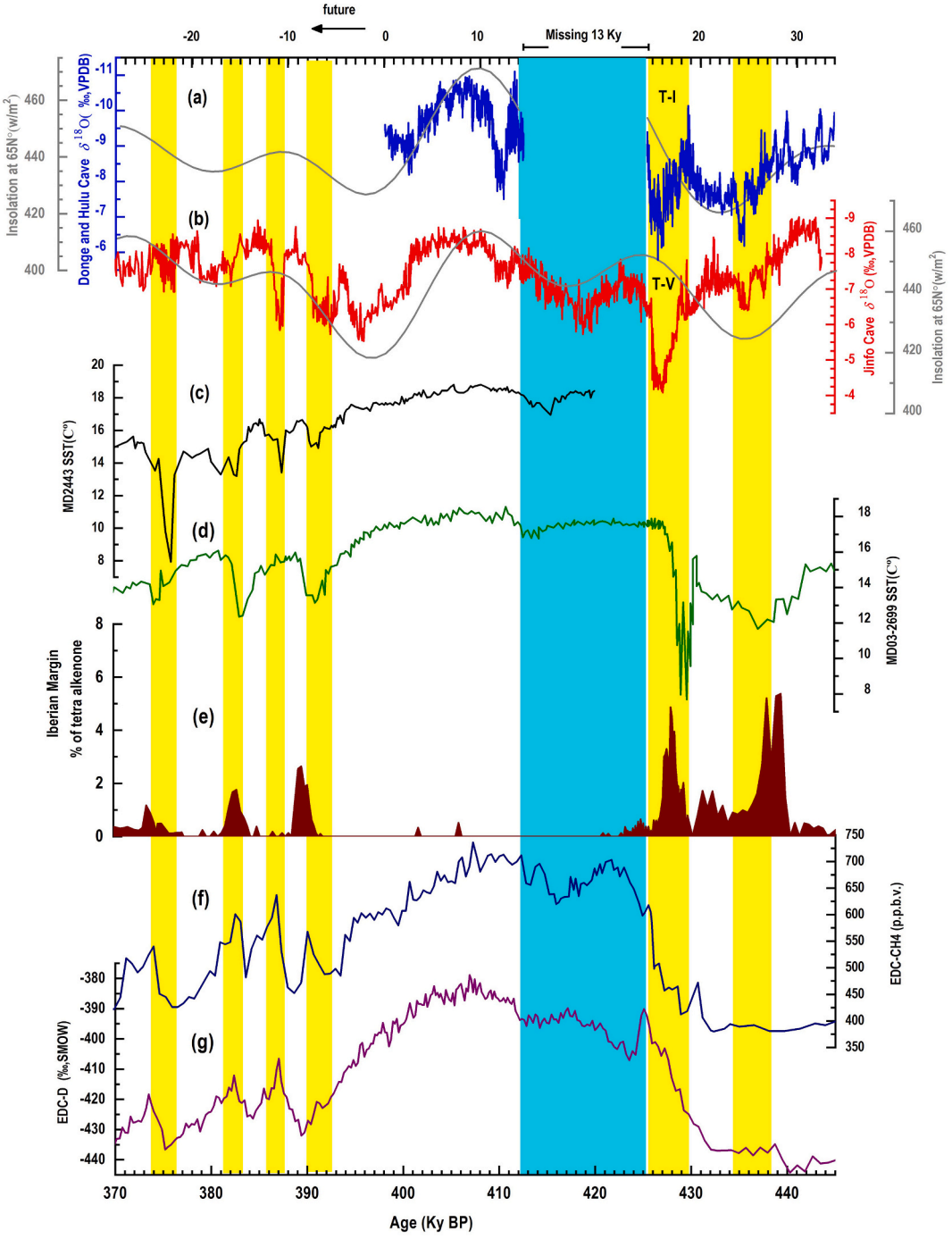

Fig. 5. Alignment of the current interglacial and the 75-ky interval encompassing MIS 11c. (a) Chinese stalagmite $\delta^{18}O$ records (blue) for the past 34 ky overlapped with the curve of July 21 insolation at 65°N, extended 28 ky into the future (Laskar et al., 2004). (b) $\delta^{18}O$ record of stalagmite J33 (red) overlapped with the curve of July 21 insolation at 65°N during 370–445 ky BP. (c) Alkenone-based sea surface temperature (SST) record from core MD01–2443 (Martrat et al., 2007). (d) North Atlantic SST (U_k'37) record (Voelker et al., 2010). (e) Tetra alkenone record from the Iberian Margin (Rodrigues et al., 2011). Records of (f) methane and (g) δD from the EPICA Dome C ice core from Antarctica (EPICA community members, 2004). Yellow bars indicates millennial-scale Heinrich-type events (Voelker et al., 2010; Palumbo et al., 2013). The cyan bar indicates the missing part of MIS 1—i.e., the interval of the first 13 ky of MIS 11 has no analogue in the current interglacial (Candy et al., 2014). (For interpretation of the references to colour in this figure legend, the reader is referred to the web version of this article.)

Loutre and Berger, 2003). This difference is evident not only in astronomical orbital parameters, but also in paleoclimatic records. The high-resolution stalagmite J33 record clearly records MIS11d and MIS11e, corresponding to the first smaller precession cycle of MIS 11. However, MIS 1 lacks the intervals corresponding to MIS11d and MIS11e—in other words, the first 13 ky (MIS 11d and MIS 11e) of MIS 11 have no analogue in the Holocene (Candy et al., 2014). Therefore, this 13 ky interval is regarded as a missing part of the Holocene rather than a predictor of what will happen in the future, which also explains why the MIS 11 interglacial period was longer than the current interglacial period. Conventionally, it is difficult to distinguish MIS 11c, MIS 11d and MIS 11e in many geological archives (Bassinot et al., 1994; Mcmanus et al., 1999; Dickson et al., 2009; Melles et al., 2012; Markovic et al., 2011), and for this reason researchers often regard the end of T-V

as the beginning of MIS 11c, and the first part of MIS 11 (425–397 ky BP) is collectively referred to as MIS 11c or MIS 11.3, thus comprising a prolonged interglacial period. The low-latitude monsoon that responds to precession shows obvious phases corresponding to MIS 11d and MIS 11e, enabling us to estimate the true duration of MIS 11c. Kukla (2003) questioned whether the first part of MIS 11 can be interpreted as a true interglacial period, or whether MIS 11 lacks the cold phase corresponding to MIS5d. According to the stalagmite J33 record, there was a weak monsoon phase (MIS 11d) in the early part of MIS 11, corresponding to MIS5d, which interrupted the strengthening trend of the monsoon in the early stage of MIS 11.

This new alignment strategy shows that the period of 400–365 ky BP can provide a reference for signs of glacial inception in the future, with the unusually long MIS 11 interglacial ending at about 396 ± 3 ky BP, coinciding with the timing of the insolation minimum. However, this alignment, based primarily on the orbital parameters of the two phases and the similarity of the stalagmite records, may underestimate the role of the insolation threshold required to initiate a glaciation (Yin et al., 2021). The insolation minimum of ~2 ky AP is greater than the insolation minimum at ~397 ky BP. Even if the insolation threshold for glacial inception was reached at ~397 ky, it is unclear that it was reached either at the present-day or at ~2 ky AP. The latest simulation shows that the current interglacial will be exceptionally long, and that the next glacial inception would not occur until 50 ky in the future, because the insolation minima remain high (Ganopolski et al., 2016;Yin et al., 2021). Given our understanding of interglacial diversity, there is clearly no reason to believe that the climate of the remainder of MIS 1 will replicate the structure of MIS 11, or last for the same length of time, although there are close similarities in insolation forcing (Yin & Berger, 2015). However, MIS 11 is still a critical time interval for understanding the current interglacial period and predicting its future course, and it is the only interglacial period driven by both high greenhouse gas concentrations and low eccentricity- related insolation characteristics.

Indeed, atmospheric CO_2 plays an important role in glacial inceptions (Vettoretti and Peltier, 2004). During MIS 11c, atmospheric CO_2 concentrations remained high (~280 ppmv), equivalent to the preindustrial CO_2 level of the Holocene, which may be insufficient to trigger new ice growth given the insolation minimum (Loutre and Berger, 2000; Vettoretti and Peltier, 2004; Yin & Berger, 2010). On this basis, climate simulations have suggested that orbital forcing will not trigger glacial inception until ~50 ky AP (Ganopolski et al., 2016; Loutre and Berger, 2003). Clearly, more research is needed to resolve uncertainties regarding the thresholds (i.e., insolation, greenhouse gases, and internal feedbacks) required to initiate a glacial inception.

5. Conclusions

MIS 11 remains a crucial time interval for investigating processes and events that are fundamental to our understanding of the impact of anthropogenic greenhouse warming. From the perspective of the Asian monsoon, we used stalagmite $\delta^{18}O$ records to determine the utility of MIS 11 as an analog of the current interglacial period. The stalagmite $\delta^{18}O$ record from Jinfo Cave, near Chongqing in Southwest China, shows that MIS 11 can be divided into 5 stages, suggesting that the monsoon was the strongest and most stable during MIS 11c, which was the climatic optimum of MIS 11. We developed a new alignment strategy based on precession (insolation maximum) and the preceding termination, and found that MIS 11d and MIS 11e together lasted for ~13 ky, which has no analogue in the current interglacial. A corollary of our alignment is that the period of 400–365 ky BP can provide a reference for signs of glacial inception in the future, however, considering the insolation threshold and the impact of human activities, many uncertainties remain regarding the timing of the onset of the next ice age.

Data and materials availability

All data needed to evaluate the conclusions in the paper are given in the paper and/or the Supplementary Materials. Additional data related to this paper may be requested from the authors.

Acknowledgments and data

This research was supported by National Natural Science Foundation of China (41971109, 41931178, 41572158, 41571102, and 41572340); Innovation Research 2035 Pilot Plan of Southwest University (SWU-XDZD22003); U—Th dating at the HISPEC was supported by grants from the Science Vanguard Research Program of the Ministry of Science and Technology (MOST) (109-2123-M-002-001 to C.-C.S.), the National Taiwan University (109L8926 to C.-C.S.), the Higher Education Sprout Project of the Ministry of Education, Taiwan ROC (109L901001 to C.-C. S.). The stalagmite $\delta^{18}O$ data and chronological data used to support the findings of this study can be obtained in the supporting information file (available online). All these data will be deposited in the World Data Center repository (https://www.ncdc.noaa.gov/data-access/paleoclimatology-data/datasets/speleothem).

Declaration of Competing Interest

We declare that we do not have any commercial or associative interest that represents a conflict of interest in connection with the work submitted.

Data availability

I have shared the link to my data at the Attach File step.

Appendix A. Supplementary data

Supplementary data to this article can be found online at https://doi.org/10.1016/j.palaeo.2022.111311.

References

Bassinot, F.C., Labeyrie, L.D., Vincent, E., Quidelleur, X., Shackleton, N.J., Lancelot, Y., 1994. The astronomical theory of climate and the age of the Brunhes-Matuyama magnetic reversal. Earth Planet. Sci. Lett. 126 (1–3), 91–108. https://doi.org/10.1016/0012-821X(94)90244-5.

Mills, Benjamin J.W., Otto-Bliesner, Bette L., Ridgwell, Andy, ZhangGavin, Yi Ge, Foster, L., Goddéris, Yves, Huber, Brian T., Ivany, Linda C., Turner, Sandra Kirtland, Lunt, Daniel J., McElwain, Jennifer C., Hönisch, Gordon N., Inglis, Sierra V., Petersen, Navjit Sagoo, Tabor, Clay R., Thirumalai, Kaustubh, Zhu, Jiang, Burls, Natalie J., Tierney, Jessica E., Poulsen, Christopher J., Montañez, Isabel P., Bhattacharya, Tripti, Feng, Ran, Ford, Heather L., Bärbel., 2020. Past climates inform our future. Science 370 (6517), eaay3701. https://doi.org/10.1126/science.aay3701.

Broecker, W.S., 1998. Paleocean circulation during the last Deglaciation: a bipolar seesaw? Paleoceanography 13, 119–121. https://doi.org/10.1029/97PA03707.

Candy, I., Schreve, D.C., Sherriff, J., Tye, G.J., 2014. Marine Isotope Stage 11: Palaeoclimates, palaeoenvironments and its role as an analogue for the current interglacial. Earth Sci. Rev. 128 (18–51), 0012–8252. https://doi.org/10.1016/j.earscirev.2013.09.006.

Chen, C.J., Li, T.Y., 2018. Geochemical characteristics of cave drip water respond to enso based on a 6-year monitoring work in yangkou cave, Southwest China. J. Hydrol. 561, 896–907. https://doi.org/10.1016/j.jhydrol.2018.04.061.

Cheng, H., Zhang, H., Cai, Y., Shi, Z., Yi, L., Deng, C., Hao, Q., Peng, Y., Sinha, A., Li, H., Zhao, J., Tian, Y., Baker, J., Perez-Mejías, C., 2021. Orbital-scale Asian summer monsoon variations: paradox and exploration. Sci. China Earth Sci. 64 (4), 529–544. https://doi.org/10.1007/s11430-020-9720-y.

Cheng, H., Zhang, H., Zhao, J., et al., 2019. Chinese stalagmite pale H oclimate researches: a review and perspective. Sci. China Earth Sci. 1–25.

Cheng, H., Edwards, R.L., Shen, C.C., Polyak, V.J., Asmerom, Y., Woodhead, J., et al., 2013. Improvements in 230Th dating, 230Th and 234U half-life values, and U-Th isotopic measurements by multi-collector inductively coupled plasma mass spectrometry. Earth Planet. Sci. Lett. 371–372, 82–91. https://doi.org/10.1016/j.epsl.2013.04.006.

Cheng, H., Edwards, R.L., Sinha, A., Spötl, C., Yi, L., Chen, S., et al., 2016. The asian monsoon over the past 640,000 years and ice age terminations. Nature 534 (7609), 640–646. https://doi.org/10.1038/nature18591.

Clemens, S.C., Holbourn, A., Kubota, Y., Lee, K.E., Liu, Z., Chen, G., et al., 2018. Precession-band variance missing from East asian monsoon runoff. Nat. Commun. 9 (1), 3364. https://doi.org/10.1038/s41467-018-05814-0.

de Abreu, F.F., Abrantes, N.J., Shackleton, P.C., Tzedakis, J.F., McManus, D.W., Oppo, M. A.Hall, 2005. Ocean climate variability in the eastern North Atlantic during interglacial marine isotope stage 11: a partial analogue to the Holocene? Paleoceanography 20, PA3009.

Denton, G.H., Anderson, R.F., Toggweiler, J.R., Edwards, R.L., Schaefer, J.M., Putnam, A. E., 2010. The last glacial termination. Science 328 (5986), 1652–1656. https://doi.org/10.1126/science.1184119.

Dickson, A.J., Beer, C.J., Dempsey, C., Maslin, M.A., Bendle, J.A., Mcclymont, E.L., Pancost, R.D., 2009. Oceanic forcing of the Marine Isotope Stage 11 interglacial. Nat. Geosci. 2 (6), 428–433. https://doi.org/10.1038/ngeo527.

Dorale, J., Liu, Z., 2009. Limitations of Hendy Test criteria in judging the paleoclimatic suitability of speleothems and the need for replication. J. Cave. Karst. Stud. 71, 73–138.

EPICA community members, 2004. Eight glacial cycles from an Antarctic ice core. Nature 429, 623–628.

Ganopolski, A., Winkelmann, R., Schellnhuber, H.J., 2016. Critical insolation-CO2 relation for diagnosing past and future glacial inception. Nature 529 (7585), 200–203. https://doi.org/10.1038/nature16494.

Hendy, C.H., 1971. The isotopic geochemistry of speleothems—I. The calculation of the effects of different modes of formation on the isotopic composition of speleothems and their applicability as palaeoclimatic indicators. Geochem. Cosmochim. Acta 35, 801–824.

Huybers, P., Wunsch, C., 2005. Obliquity pacing of the late Pleistocene glacial terminations. Nature 434 (7032), 491–494. https://doi.org/10.1038/nature03401.

Imbrie, J., Shackleton, N.J., Pisias, N.G., Morley, J.J., Prell, W.L., Martinson, D.G., et al., 1984. The orbital theory of Pleistocene climate: support from a revised chronology of the marine δ18O record. In: Milankovitch and Climate: Understanding the Response to Astronomical Forcing, pp. 269–305. https://ui.adsabs.harvard.edu/abs/1984mcur.conf.269I.

Jaffey, A.H., Flynn, K.F., Glendenin, L.E., Bentley, W.C., Essling, 1971. A. M. Precision measurement of half-lives and specific activities of 235U and 238U. Phys. Rev. C 4, 1889–1906.

Jouzel, J., Masson-Delmotte, V., Cattani, O., Dreyfus, G., Falourd, S., Hoffmann, G., et al., 2007. Orbital and millennial Antarctic climate variability over the past 800,000 years. Science 317 (5839), 793–796. https://doi.org/10.1126/science.1141038.

Kandiano, E.S., van der Meer, M.T.J., Schouten, S., Fahl, K., Sinninghe Damsté, J.S., Bauch, H.A., 2017. Response of the North Atlantic surface and intermediate ocean structure to climate warming of MIS 11. Sci. Rep. 7, 46192. https://doi.org/10.1038/srep46192.

Koutsodendris, A., Müller, U.C., Pross, J., Brauer, A., Kotthoff, U., Lotter, A.F., 2010. Vegetation dynamics and climate variability during the Holsteinian interglacial based on a pollen record from Dethlingen (northern Germany). Quat. Sci. Rev. 29 (23–24), 3298–3307. https://doi.org/10.1016/j.quascirev.2010.07.024.

Kukla, G., 2003. Continental records of MIS 11. In: Droxler, A.W., Poore, R.Z., Burckle, L. H. (Eds.), Earth's Climate and Orbital Eccentricity: The Marine Isotope Stage 11 Question, Geophysical Monograph Series, 137, pp. 207–212.

Laskar, J., et al., 2004. A long-term numerical solution for the insolation quantities of the Earth. Astron. Astrophys. 428, 61–285.

Lisiecki, L.E., Raymo, M.E., 2005. A Pliocene-Pleistocene stack of 57 globally distributed benthic δ18O records. Paleoceanography 20 (1), PA1003. https://doi.org/10.1029/2004PA001071.

Loutre, M.F., Berger, A., 2000. Future climatic changes: are we entering an exceptionally long interglacial? Clim. Chang. 46, 61–90. https://doi.org/10.1023/A:1005559827189.

Loutre, M.F., Berger, A., 2003. Marine Isotope Stage 11 as an analogue for the present interglacial. Glob. Planet. Chang. 36 (3), 209–217. https://doi.org/10.1016/S0921-8181(02)00186-8.

Maher, B.A., 2008. Holocene variability of the East asian summer monsoon from chinese cave records: a re-assessment. The Holocene 18 (6), 861–866. https://doi.org/10.1177/0959683608095569.

Markovic, S.B., Hambach, U., Stevens, T., Kukla, G.J., Heller, F., McCoy, W.B., et al., 2011. The last million years recorded at the Stari Slankamen loess–palaeosol sequence: revised chronostratigraphy and long-term environmental trends. Quat. Sci. Rev. 30 (9–10), 1142–1154. https://doi.org/10.1016/j.quascirev.2011.02.004.

Martrat, B., Grimalt, J.O., Shackleton, N.J., de Abreu, L., Hutterli, M.A., Stocker, T.F., 2007. Four climate cycles of recurring deep and surface water destabilizations on the Iberian margin. Science 317, 502–507. https://doi.org/10.1126/science.1139994.

Masson-Delmotte, V., Valerie, Dreyfus, Gabrielle, Braconnot, P., Johnsen, S., 2006. Past temperature reconstructions from deep ice cores: relevance for future climate change. Clim. Past 2, 145–165. https://doi.org/10.5194/cp-2-145-2006.

Mcmanus, J., Oppo, D.W., Cullen, J.L., 1999. A 0.5-million-year record of millennial-scale climate variability in the North Atlantic. Science 283 (5404), 971–975. https://doi.org/10.1126/science.283.5404.971.

Melles, M., Brigham-Grette, J., Minyuk, P.S., Nowaczyk, N.R., Wennrich, V., DeConto, R. M., et al., 2012. 2.8 million years of Arctic climate change from Lake El'gygytgyn, NE Russia. Science 337 (6092), 315–320. https://doi.org/10.1126/science.1222135.

Palumbo, E., Flores, J.A., Perugia, C., Petrillo, Z., Voelker, A.H.L., Amore, F.O., 2013. Millennial scale coccolithophore paleoproductivity and surface water changes between 445 and 360 ka (Marine Isotope Stages 12/11) in the Northeast Atlantic. Palaeogeogr. Palaeoclimatol. Palaeoecol. 383–384, 27–41. https://doi.org/10.1016/j.palaeo.2013.04.024.

Prokopenko, A.A., Karabanov, E.B., Williams, D.F., Kuzmin, M.I., Shackleton, N.J., Crowhurst, S.J., et al., 2001. Biogenic Silica Record of the Lake Baikal Response to Climatic Forcing during the Brunhes. Quat. Res. 55 (2), 123–132. https://doi.org/10.1006/qres.2000.2212.

Railsback, L.B., Gibbard, P.L., Head, M.J., Voarintsoa, Ny Riavo, G., amp, Toucanne, S., 2015. An optimized scheme of lettered marine isotope substages for the last 1.0 million years, and the climatostratigraphic nature of isotope stages and substages. Quat. Sci. Rev. 111, 94–106. https://doi.org/10.1016/j.quascirev.2015.01.012.

Rodrigues, T., Antje, V., Joan, G., Fatima, A., Filipa, N., 2011. Iberian margin sea surface temperature during MIS 15 to 9 (580–300 ka): Glacial suborbital variability versus interglacial stability. Paleoceanography 26. https://doi.org/10.1029/2010pa001927.

Ruddiman, W.F., 2005. Cold climate during the closest stage 11 analog to recent Millennia. Quat. Sci. Rev. 24 (10–11), 1111–1121. https://doi.org/10.1016/j.quascirev.2004.10.012.

Ruddiman, W.F., 2007. The early Anthropogenic hypothesis: challenges and responses. Rev. Geophys. 45, 1–37. https://doi.org/10.1029/2006RG000207.

Shen, C.-C., Wu, C.-C., Cheng, H., et al., 2012. High-precision and highresolution carbonate 230Th dating by MC-ICP-MS with SEM protocols. Geochim. Cosmochim. Acta 99, 71–86.

Siddall, M., Rohling, E.J., Blunier, T., Spahni, R., 2010. Patterns of millennial variability over the last 500 ka. Clim. Past 6, 295–303. https://doi.org/10.5194/cp-6-295-2010.

Stephen, Barker, Paula, Diz, Maryline, J., Vautravers, et al., 2009. Interhemispheric Atlantic seesaw response during the last deglaciation. Nature 457 (7233), 1097–1102. https://doi.org/10.1038/nature07770.

Tan, M., 2009. Circulation effect: climatic significance of the short term variability of the oxygen isotopes in stalagmites from monsoonal China. Quat. Sci. 29 (5), 851–862 (in Chinese with English abstract).

Tierney, J.E., Poulsen, C.J., Montañez, I.P., Bhattacharya, T., Feng, R., Ford, H.L., et al., 2020. Past climates inform our future. Science 370 (6517), eaay3701. https://doi.org/10.1126/science.aay3701.

Tzedakis, P.C., 2010. The MIS 11 – MIS 1 analogy, southern european vegetation, atmospheric methane and the "early anthropogenic hypothesis". Clim. Past Discuss. 6, 131–144. http://www.clim-past-discuss.net/5/1337/2009/cpd-5-1337-2009.

Tzedakis, P.C., Crucifix, M., Mitsui, T., Wolff, E.W., 2017. A simple rule to determine which insolation cycles lead to interglacials. Nature 542, 427–432. http://www.nature.com/doifinder/10.1038/nature21364.

Tzedakis, P.C., Wolff, E.W., Skinner, L., Brovkin, V., Hodell, D.A., McManus, J., Dominique, R., 2012. Can we predict the duration of an interglacial? Clim. Past 8, 1057–1088. https://doi.org/10.5194/cpd-8-1057-2012.

Vettoretti, G., Peltier, W.R., 2004. Sensitivity of glacial inception to orbital and greenhouse gas climate forcing. Quat. Sci. Rev. 23 (3–4), 499–519. https://doi.org/10.1016/j.quascirev.2003.08.008.

Voelker, A.H.L., Rodrigues, T., Billups, K., Oppo, D., McManus, J., Stein, R., Hefter, J., Grimalt, J.O., 2010. Variations in mid-latitude North Atlantic surface water properties during the mid-Brunhes (MIS 9–14) and their implications for the thermohaline circulation. In: Climate of the Past (CP) & Discussions (CPD), 6, pp. 531–552. http://www.clim-past.net/6/531/2010/cp-6-531-2010.

Wang, Y.J., Cheng, H., Edward, R.L., 2001. A high-resolution absolute-dated late Pleistocene Monsoon record from Hulu Cave, China. Science 294, 2345–2348.

Wang, Y.J., Cheng, H., Edwards, R.L., Kong, X.G., Shao, X.H., Chen, S.T., et al., 2008. Millennial-and Orbital-scale changes in the East Asian Monsoon over the past 224,000 years. Nature 451, 1090–1093. https://doi.org/10.1038/nature06692.

Yang, X.L., Yang, H., Wang, B.Y., et al., 2019. Early-Holocene monsoon instability and climatic optimum recorded by chinese stalagmites. The Holocene 29 (6), 1059–1067.

Yin, Q.Z., Wu, Z.P., Berger, A., et al., 2021. Insolationtriggered abrupt weakening of Atlantic circulation at the end of interglacials. Science 373, 1035–1040. http://www.science.org/doi/epdf/10.1126/science.abg1737.

Yin, Q., Berger, A., 2010. Insolation and CO2 contribution to the interglacial climate before and after the Mid-Brunhes Event. Nat. Geosci. 3 (4), 243–246.

Yin, Q., Berger, A., 2015. Interglacial analogues of the Holocene and its natural near future. Quat. Sci. Rev. 120, 28–46. https://doi.org/10.1016/j.quascirev.2015.04.008.

Yuan, D.X., Cheng, H., Edwards, R., et al., 2004. Timing, duration, and transitions of the last interglacial asian monsoon. Science 304 (23), 575–578.

Zhang, P.Z., Cheng, H., Edwards, R.L., et al., 2008. A test of climate, sun, and culture relationships from an 1810-year chinese cave record. Science 322, 940–942.

Zhao, X., Cheng, H., Sinha, A., Zhang, H., Baker, J.L., Chen, S., et al., 2019. A high-resolution speleothem record of Marine Isotope Stage 11 as a natural analog to Holocene asian summer monsoon variations. Geophys. Res. Lett. 46, 9949–9957. https://doi.org/10.1029/2019GL083836.